Naval Research Laboratory

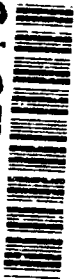Washington, DC 20375-5000

AD-A256 056

Opacity, Equation of State, and Radiation Transport Model for Moderate Density, eV-Temperature Plasmas

J. P. Apruzese, J. L. Giuliani, Jr., and P. C. Kepple

Radiation Hydrodynamics Branch
Plasma Physics Division

September 22, 1992

DTIC
SELECTE
OCT 0 6 1992
B

92 1

1. AGENCY USE ONLY *(Leave Blank)*	2. REPORT DATE September 22, 1992	3. REPORT TYPE AND DATES COVERED Interim	
4. TITLE AND SUBTITLE Opacity, Equation of State, and Radiation Transport Model for Moderate Density, eV-Temperature Plasmas			5. FUNDING NUMBERS PE - 63220C
6. AUTHOR(S) John P. Apruzese, John L. Giuliani, Jr., and Paul C. Kepple			
7. PERFORMING ORGANIZATION NAME(S) AND ADDRESS(ES) Naval Research Laboratory Washington, DC 20375-5320			8. PERFORMING ORGANIZATION REPORT NUMBER NRL/MR/4721—92-7124
9. SPONSORING/MONITORING AGENCY NAME(S) AND ADDRESS(ES) SDIO Pentagon Washington, DC 20301-7100			10. SPONSORING/MONITORING AGENCY REPORT NUMBER

11. SUPPLEMENTARY NOTES

This work was performed by the Radiation Hydrodynamics Branch, Plasma Physics Division for the Strategic Defense Initiative Organization under Job Order Title, Ultra Short Wavelength Laser Research, Program Element 63220C.

12a. DISTRIBUTION/AVAILABILITY STATEMENT Approved for public release; distribution is unlimited.	12b. DISTRIBUTION CODE

13. ABSTRACT *(Maximum 200 words)*

We present a model suitable for calculating opacity and radiation transport in eV-temperature plasmas such as those encountered in electromagnetic launchers, arcjets, and some types of plasma processing. Using a detailed multilevel, atomic model, the opacity at about 1400 frequency points is calculated for a grid of temperature and electron densities using either the LTE or CRE approximation. This detailed grid is further simplified to 15-20 energy bins within each of which the Planck mean opacity is calculated and stored for use by a radiation transport code. This radiation transport model is a quasi-two-dimensional ray trace at each of these bins suitable for rapid calculation of approximate radiative cooling (heating) for use in conjunction with a hydrodynamics model.

14. SUBJECT TERMS		15. NUMBER OF PAGES 20
Radiation transport Planck mean opacity	Electromagnetic launchers Local thermodynamic equilibrium	16. PRICE CODE

17. SECURITY CLASSIFICATION OF REPORT UNCLASSIFIED	18. SECURITY CLASSIFICATION OF THIS PAGE UNCLASSIFIED	19. SECURITY CLASSIFICATION OF ABSTRACT UNCLASSIFIED	20. LIMITATION OF ABSTRACT SAR

CONTENTS

iii

OPACITY, EQUATION OF STATE, AND RADIATION TRANSPORT MODEL FOR MODERATE DENSITY, eV-TEMPERATURE PLASMAS

I. Introduction

Historically, a principal interest of the Radiation Hydrodynamics Branch has been dense, highly ionized plasmas. Such plasmas have temperatures in the hundred-eV to kilovolt range, and are typically stripped to or near the K shell for atomic numbers Z $\leq$ 20, or the L shell for mid- range atomic numbers. They are of considerable interest in such areas as fusion, weapons effects simulation, and development of x-ray lasers. The bulk of the Branch's modeling capability has been shaped and tailored to meet the difficult challenge of calculating the radiation hydrodynamics and interpreting the emissions of such media.

However, interest in much cooler, more weakly ionized plasmas has heightened recently due to their presence and application in the rapidly developing areas of plasma processing[1] (including arcjets[2]) and electromagnetic launchers.[3] In many instances, these media do not possess either the symmetry or uniformity associated with higher temperature plasmas, such as spherically compressed pellets or exploded-foil x-ray lasers. This complicates the task of modeling. However, a compensating simplification is present in that most if not all of these plasmas can be adequately described by the local thermodynamic equilibrium approximation (LTE). This is almost never true of their high temperature counterparts.

In the succeeding sections we describe the individual facets of a model which provides highly efficient calculation of charge state, internal energy, opacity, and radiation transport for use in conjunction with hydrodynamics calculations of the evolution and properties of such plasmas. In Sec. II, the basic atomic data and its storage are covered. In Sec. III, we describe the calculation of charge state, internal energy, and opacity in both LTE and CRE cases as well as the comparison of results from these two assumptions. Finally, in Sec. IV, the radiation transport model which makes use of the stored opacities is developed.

II. Atomic Data and Storage

The fundamental quantities of interest are the charge state, internal energy per ion, and absorption coefficient for a given element as a function of plasma temperature, photon energy, and electron density. Electron, rather than total ion density ,is chosen as

an independent variable because these plasmas in general may contain several different elements which each contribute electrons. At the end of each hydrodynamic time step, mutually consistent values for electron density and temperature are determined from the tables assuming that total internal energy (i.e., thermal plus ionization and excitation) is conserved. The electron density is obtained as the sum of the density of each ion species times its charge.

To calculate the plasma's average charge state and internal energy per ion, one need not know the detailed atomic rates if the plasma is in LTE. In such a situation, where collisional rates dominate radiative decay, the population ratio of two levels within a single ionization stage is given by the well-known Boltzmann distribution

$$\frac{N_i}{N_j} = \frac{g_i}{g_j} e^{\frac{-E_{ij}}{T}}. \tag{1}$$

where the g's are the levels' statistical weights and E_{ij} and T the level separation and temperature in eV, respectively. For levels in adjacent ionization stages, their ratio is determined by the Saha equation

$$\frac{N_1}{N_0} = \frac{g_1}{g_0} \frac{6.04 \times 10^{21}}{N_e} T^{1.5} e^{\frac{-\chi}{T}} \tag{2}$$

where N_e is the total electron density (cm^{-3}), 1 is the more highly ionized state, and χ is the ionization energy in eV between states 0 and 1. Since it is obvious that no atomic rates occur in eq. (2) and eq. (1) it is reasonable to question the need for such rates for an LTE plasma. There are two factors which argue strongly for the calculation and availability of such rates: first, the need to know opacity, which depends on line broadening which in turn depends in part on collisional rates, and, second, the need to check the range of validity of the LTE approximation, which requires collisional- radiative equilibrium calculations using atomic rates.

Therefore, the fundamental data upon which our calculations of charge state, internal energy, and opacity are based consists of a complete atomic table including all appropriate radiative and collisional rates connecting the levels. Collisional rates, of course, include ionization and 3-body and dielectronic recombination. A more complete description and methodology is given elsewhere .[4]

The structure of this table has been reformulated to provide for much greater efficiency and economy in both the storage and retrieval of data. The vast bulk of the rate tables produced previously by the Branch were intended for use with much hotter, more highly ionized plasmas where stripping to the K shell was guaranteed or well within the realm of possibility. These tables always included the bare nucleus and K shell; the bare nucleus itself was labelled state No. 1, the hydrogenic ground state, No. 2, etc. The computer codes that read these tables had these labellings assumed and built into their structure. While simple and efficient for the highly ionized plasmas, such a structure becomes quite wasteful if one is interested in, say, copper (atomic number 29), at temperatures of 1-5 eV, where only the first few ionization stages will be present. Reserving space for the ~ 25 ionization stages which will not be present clearly makes no sense.

The tabular arrangement used in the present work makes use of an "equivalent bare nucleus" whose number of electrons is given by the integer LNGS-1. This is labelled state No. 1. For instance, consider boron (Z=5) which we use as an example throughout the remainder of this report. If LNGS=2, for example, the hydrogenic ground state is equivalent to the bare nucleus, i.e., no more highly ionized states are carried in the table. It is up to the user to check that this is consistent with the expected plasma temperatures. There are other individual integers stored at the beginning of the table which denote the first and last ionization stages with structure, and the most neutral ground state. Therefore, nearly complete flexibility can be obtained with almost no wasted storage space. Furthermore, readability of the table for use in analysis is greatly improved by the recapitulation of the temperature before each block of rates as well as the clear listing of the spectroscopic notation for each level in "A" format at the beginning of the file. *Within* each ionization stage, the ordering of the rates and numbering of the levels is unchanged from the old format. This new system does not require that the neutral stage be carried, that is, an "equivalent neutral state" is allowed whose number of electrons is denoted by the stored integer KNGS. This gives even more versatility as one can imagine cases where expected temperatures are sufficiently high that few neutrals are present. All results given below were obtained using a boron table constructed according to this new and considerably more efficient scheme.

3

III. Equation of State and Opacity

In the present work, we apply the term "equation of state" to mean the determination of the mean charge state and internal energy per ion as a function of electron density and temperature for a given element. No attempt is made to accomodate the physics of degeneracy or continuum lowering. The charge state and internal energy are determined, of course, by the populations of the various ground and excited levels. In calculating those populations, we first seek to determine whether the greatly simplifying approximation of LTE is accurate for eV plasmas. We chose boron as a test case for these plasma calculations where only the first three ionization states are expected to be present. A temperature range of 0.3-4.0 eV and ion densities down to 10^{16} cm^{-3} were thoroughly explored by computing and comparing the level populations in both CRE and LTE.

The atomic model employed for boron ions includes the ground states from neutral through hydrogenic, as well as 5 excited states for the neutral species, 9 for the singly ionized state, and 7 in the doubly ionized Li-like stage, for a total of 26 levels. In addition to solving for the level populations, a detailed calculation of boron's absorption coefficient at each of the temperature-density points was performed. This opacity calculation utilized a grid of 1400 separate energy points ranging from 1 to 50 eV. Each spectral line in this energy range is given a Voigt absorption profile whose width is determined self-consistently from the radiative and collisional rates affecting the upper and lower levels of the transition. A total of 49 lines and 19 bound-free continuum transitions are included, as well as free-free absorption using the Gaunt factors of Karzas and Latter.[5]

It is well known that, in order for LTE to be a good approximation, the collisional rates connecting the levels must well exceed the strongest radiative decay rates, thus imposing a lower limit on the electron density needed for this to occur. The dominant scaling of collisional rate coefficients with ionic charge is Z^{-3}, for radiative decay, Z^4. It is easily seen that the scaling of the collisional to radiative rate ratio (Z^{-7}) indicates that compensating electron densities must scale rapidly upward (Z^7) as the plasma temperature and ionic charge increase, to keep LTE valid. A previous detailed investigation[6] showed that aluminum (Z=13) ions stripped to the K shell require electron densities of 10^{25} for

4

LTE to be a valid approximation. Working backwards, a typical singly ionized species would need an electron density of only $\sim \frac{10^{25}}{13T} \sim 10^{17}$ cm^{-3} for LTE to be valid.

The present results are consistent with this estimate. For boron ion densities above 10^{17}cm^{-3} (electron density is of the same order), no significant differences between LTE and CRE populations were found. Only for the lowest ion density (10^{16}cm^{-3}) did serious differences appear. For instance, at 4 eV, at this density, the LTE approximation predicts that 97% of the boron ions will be in the He-like stage, whereas CRE yields 73%. A few of the excited state populations differ by an order of magnitude. Both the detailed nature of the opacity calculation and the effect of the CRE vs. LTE assumptions are illustrated in Figs. 1 and 2, where one notes that differences in absorption coefficient are minimal, but they become more pronounced at higher energies. Only at energies greater than 20 eV, where a 4 eV Planckian emits just 24% of its energy, do the continuum absorption coefficients differ appreciably. Given the demonstrated wide applicability of the LTE approximation for these eV-temperature plasmas, we have adopted this assumption in obtaining the results described below. At this date, comprehensive tables of the mean charge and internal energy per ion have been established for helium, boron, and aluminum using the LTE assumption.

In general, the plasma radiation hydrodynamics calculations also require a radiation transport model to provide local radiative heating (or cooling) rates within the plasma as well as heat loads on the surfaces of interest. The transport calculation itself is covered in the next section. All radiation transport algorithms, however, need an absorption coefficient (opacity) to calculate both emissivity and attenuation as a function of energy. Clearly, the direct use of all 1400 absorption coefficients from the fundamental energy grid (Figs. 1 and 2) would provide optimum accuracy, but it would also be prohibitively expensive. Use of a single mean opacity for the entire spectrum represents the other extreme; cheap but very poor results would generally be obtained. The usual solution,and the one also adopted in the present work, is a compromise in which the absorption coefficient is averaged over 10-100 energy bins for use by a transport calculation. The critical question is: which type of mean coefficient should be used?

Two varieties of mean absorption coefficient are in general use, the Rosseland and

Planck means, both described, for example, in Mihalas' textbook.[7] The Rosseland mean is the reciprocal of the weighted mean of the reciprocal of the absorption coefficient. The weighting factor is the temperature derivative of the Planck function. The Planck mean is the simple mean of the absorption coefficient weighted by the Planck function itself. As discussed in Ref. 7, the Rosseland mean gives optimum results when used with the diffusion approximation, which in turn works only for optically thick media. Since many of the plasmas of interest do not meet this criterion of large optical depth, the Rosseland mean is not an appropriate choice for the present scheme. The Planck mean absorption coefficient between energies E_0 and E_1 is given by

$$k_p = \frac{\int_{E_0}^{E_1} k_E B_E(T) dE}{\int_{E_0}^{E_1} B_E(T) dE} \tag{3}$$

where in eq. (3), k_E is the monochromatic absorption coefficient, and B the Planck function. Note that in LTE, the numerator of the above expression is the exact emission coefficient integrated between E_0 and E_1. This allows recovery of the exact optically thin result and extremely accurate cooling rates. Furthermore, if k_p is stored, this emission coefficient is obtainable if an accurate algorithm for obtaining the integral of the Planck function between two energies is available. Fortunately, a very useful rational approximation for this integral was developed by Thacher[8] and has been adopted in the present work. The Planck mean also gives the correct absorption in the optically thick limit (see Ref. 7, p.41, and Sec. IV B), and is therefore the most suitable mean opacity for use in the transport calculation. The Planck mean opacity is generally higher than the Rosseland. This is not surprising, since the Rosseland mean is a harmonic mean, weighting the low-opacity spectral regions, and the Planck is a direct mean. Fig. 3 illustrates the differences between Planck and Rosseland means for the same boron plasma conditions of Figs. 1 and 2. The spectrum from 1-50 eV has been divided into 16 energy bins each of approximately 3 eV width. Note also that in regions where spectral lines are few, the Planck and Rosseland means are nearly equal.

As a practical matter to accomodate multimaterial hydrodynamics and zonal variations in density and abundance, the opacity is stored as the base 10 logarithm of the cross section per ion in cm², for each of the 16 bins. The interval in electron density

6

is $10^{0.2}$, in temperature, $10^{0.1}$. A portion of the actual opacity table which is read by the transport routine is shown in Fig. 4.

IV. Radiation Transport

In its present realization, the radiation transport model is set up to calculate the volumetric cooling and wall loadings in a 2-D cylindrical medium where the radiative source function varies with z, the axial coordinate, as well as the radius r. There are two facets to such a calculation: (1) calculation of the specific intensity along a ray whose source function and optical depth are specified, and (2) arrangement and angle integration of the rays. These are now discussed in turn.

A. Solving the intensity along a ray

The specific intensity viewed along a ray at each grid point is given by the so-called formal solution to the transfer equation. Consider a given viewing point (called optical depth $\tau=0$, for simplicity). Viewed in the direction of the next optical depth point τ_1, the specific intensity at $\tau=0$ is

$$I_0 = I_1 e^{-\tau_1} + \int_0^{\tau_1} B(\tau) e^{-\tau} d\tau. \tag{4}$$

In eq. (4), I_1 is the intensity incident at τ_1 and $B(\tau)$ is the Planck function-the LTE source function. It is understood that this intensity applies to a specific energy, for which the subscript is suppressed for clarity. Let B_0 be the Planck function at $\tau=0$, B_1 that at τ_1. If we assume linear variation of $B(\tau)$ between these points then $B(\tau) = a + b\tau$ where $a = B_0$ and $b = \frac{(B_1-B_0)}{\tau_1}$. This linear form for $B(\tau)$, substituted into eq. (4), yields for the intensity

$$I_0 = a + b + e^{-\tau_1}(I_1 - a - b - b\tau_1). \tag{5}$$

Therefore, beginning at the far end of the ray, the intensity at any grid point may be obtained by considering each adjacent pair of points, and solving for I_0 according to eq. (5). I_0 then becomes the incident intensity (i.e., I_1) for the next pair of grid points, and the process continues until the near end of the ray is reached. This technique is amenable to very efficient programming, and can obviously be followed along either direction for a

given ray. In the initial realization of the model, the incident intensity at the ends of each ray is set to 0, i.e., the walls are assumed not to radiate and also have zero source function. We remind the reader that the optical depth is calculated using the stored Planck mean cross sections, using bilinear interpolation in temperature and electron density. The source function in each energy bin is obtained by using Thacher's[8] efficient rational approximation to the integral of the Planck function.

B. Optically thin and thick limits

Eq. (5) may be used to derive the optically thin and thick limits obtained in the present approximate scheme, verifying their correctness. Let τ_1 now be the optical depth to the surface of the medium, measured from a given interior point. If there is no incident external radiation, $I_1=0$, and eq. (5) becomes

$$I_0 = (a + b)(1 - e^{-\tau_1}) - b\tau_1 e^{-\tau_1}. \tag{6}$$

Clearly, in the limit that $\tau_1=0$, $I_0=0$ as expected, and its angular mean J, also$=0$. The net radiative cooling is given by a sum over the energy bins, of emission minus absorption, viz.

$$C_R = 4\pi \sum_{bins}(j_E - k_{pE}J_E). \tag{7}$$

In eq. (7), j_E and J_E are the emission coefficient and angular mean intensity integrated over the energy bin E. In the thin limit, $J_E =0$, therefore, the cooling rate is just $4\pi \sum_{bins} j_E$. But j_E in LTE exactly equals $k_{pE}B_E$, and since the Planck mean opacity k_{pE} and bin-integrated Planck function are in the first case stored, and in the latter case readily obtainable, the present algorithm yields the correct emission term for any LTE plasma, and therefore the exact cooling in the optically thin limit.

In the optically thick limit, eq. (6) is easily seen to yield a single angle specific intensity of $I_0 = a + b = B_0 + \frac{(B_1-B_0)}{\tau_1} \to B_0$ as $\tau_1 \to \infty$. Therefore, as expected, the angular mean intensity will approach the Planck function at each energy where the optical depth is large. As shown above, the emission portion of the net cooling is given correctly by the present technique. The absorption term in the optically thick limit where $J_E = B_E$ becomes

8

$4\pi \sum_{bins} -k_{pE}B_E$, which is exactly equal to the emission term, showing that, as expected, the net radiative cooling approaches 0 as all locally emitted radiation is locally absorbed.

C. Ray arrangement in cylindrical geometry

The initial objective in the use of the model described above is to calculate plasma cooling rates and the thermal radiative loading on the sides of a cylindrical medium whose properties vary with both z and r. In general, this requires a full two-dimensional treatment employing hundreds, perhaps thousands, of rays to fully capture all spatial variabilities of the radiation field. This may well be prohibitive when used in conjunction with hydrodynamics codes; therefore, the geometrical arrangement described below necessarily represents what is believed to be an optimal compromise between realism and efficiency.

The cylinder is divided into a number of axial zones, not necessarily of the same length. Fig. 5 shows a case of four zones. A ray is traced along the central axis, and the specific intensity along this ray is calculated at each end of the cylinder, and also in both directions at the midpoints of each axial zone. The radiative flux at each end of the cylinder is obtained by multiplying the specific intensity at each end of the ray by π, as if the radiation field were spatially isotropic. In addition to this central ray, rays are traced from the midpoint of each axial zone at r=0 to the midpoint along the wall of each zone, including the same zone, as illustrated in Fig. 5. Note in Fig. 5, only the rays emanating from zone 2 are shown for clarity. Therefore, solving the specific intensity along each of these rays provides multiangle intensity information at the axial midpoint at the radial center of each zone. The angle-averaged intensity for each energy bin is computed, which in turn allows calculation of the radiative heating term by multiplying by the local absorption coefficient and integrating over energy. Subtracting this heating factor from the cooling rate gives the net radiative heating or cooling for the zone.

At the midpoint of each axial zone along the cylinder wall, we also have multiangle intensity information since a ray has been traced there from the midpoint of each other zone as well as the local zone. The local radiative flux in an energy bin is then given by

$$F = \int_{2\pi} I(\mu)\mu d\omega \tag{8}$$

9

where μ is the cosine of the angle the ray makes with the perpendicular to the radius, and the integral extends over the 2π ster. of the hemisphere. Integrating this flux over energy then gives the local radiative heat flux to the cylinder wall.

V. Acknowledgment

VI. References

1. J. L. Shohet, Phys. Fluids B **2**, 1474 (1990).

2. A. H. Dilawari and J. Szekely, Plasma Chemistry and Plasma Processing **7**, 317 (1987).

3. D. Hahn and J. G. Gilligan, IEEE Transactions on Magnetics **27**, 251 (1991).

4. D. Duston and J. Davis, Phys. Rev. A **23**, 2602 (1981).

5. W. J. Karzas and R. Latter, Astrophys. J. Suppl. Ser. **6**, 167 (1961).

6. K. G. Whitney, J. Davis, and J. P. Apruzese, Phys. Rev. A **22**, 2196 (1980).

7. D. Mihalas, **Stellar Atmospheres**, 1st ed. (Freeman, San Francisco, 1970).

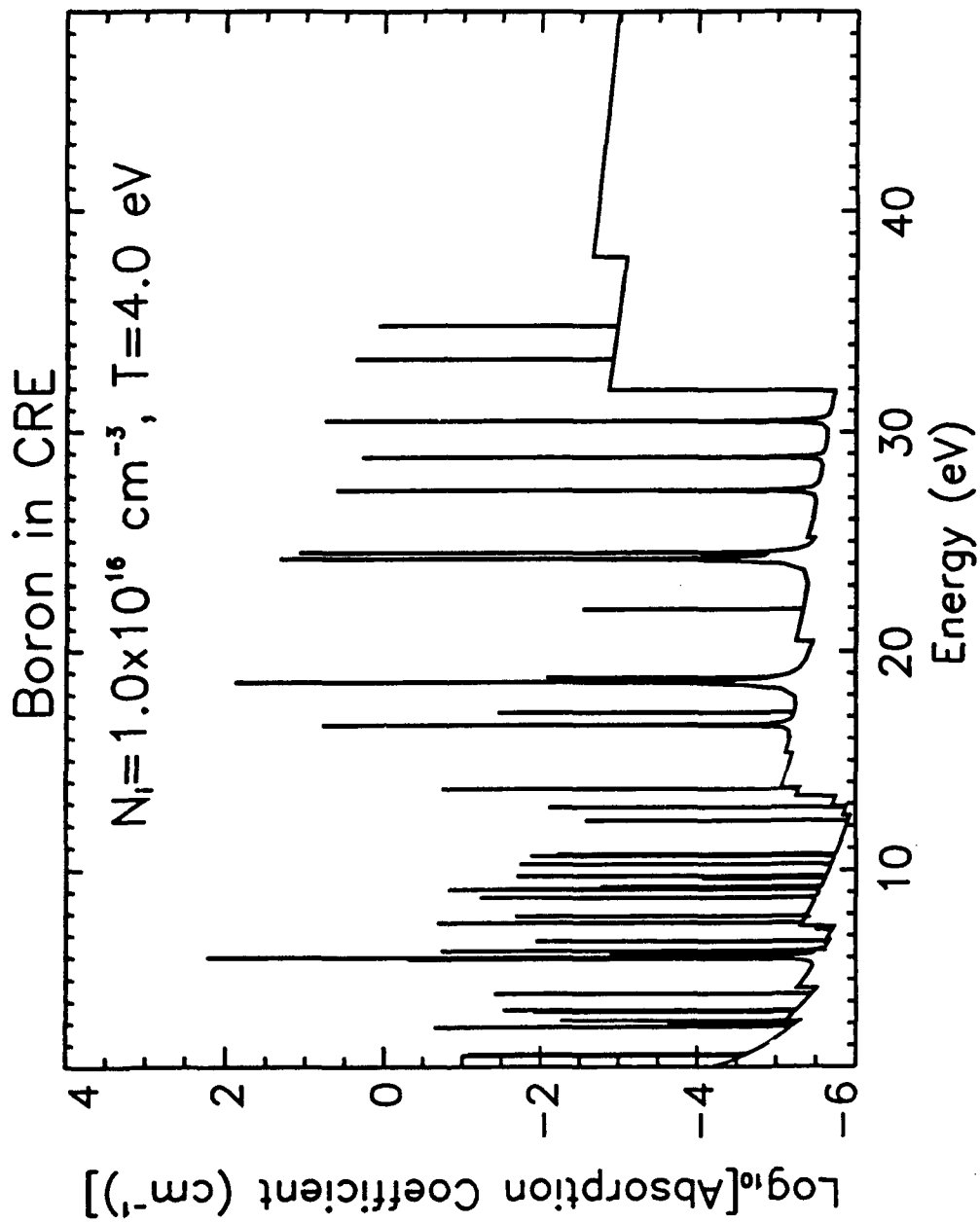8. H. C. Thacher, Jr., J. Chem. Phys. **32**, 638 (1960).

FIG. 1. Absorption coefficient for boron at total ion density of 10^{16} cm^{-3} is shown from 1-50 eV at a temperature of 4.0 eV, in CRE.
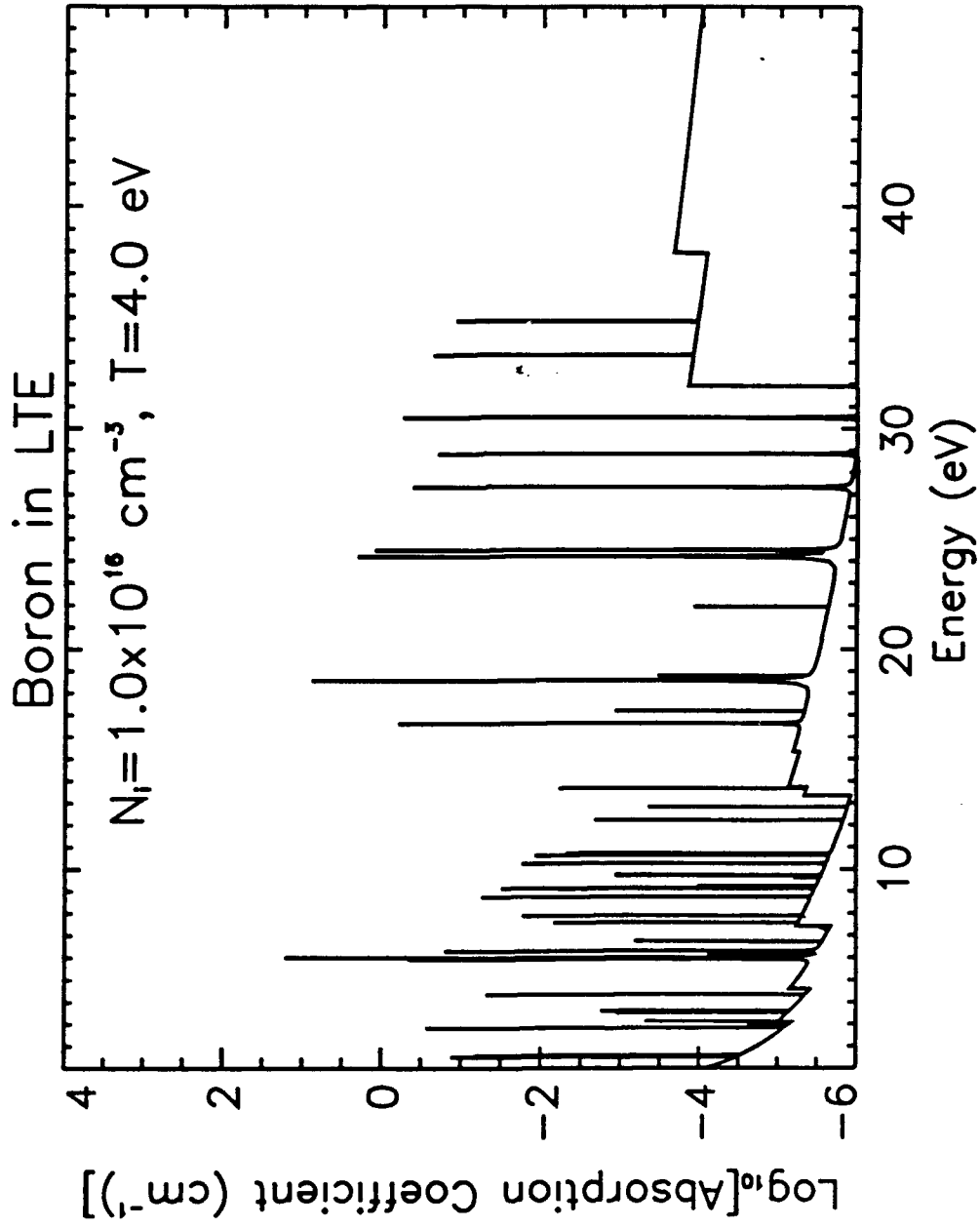
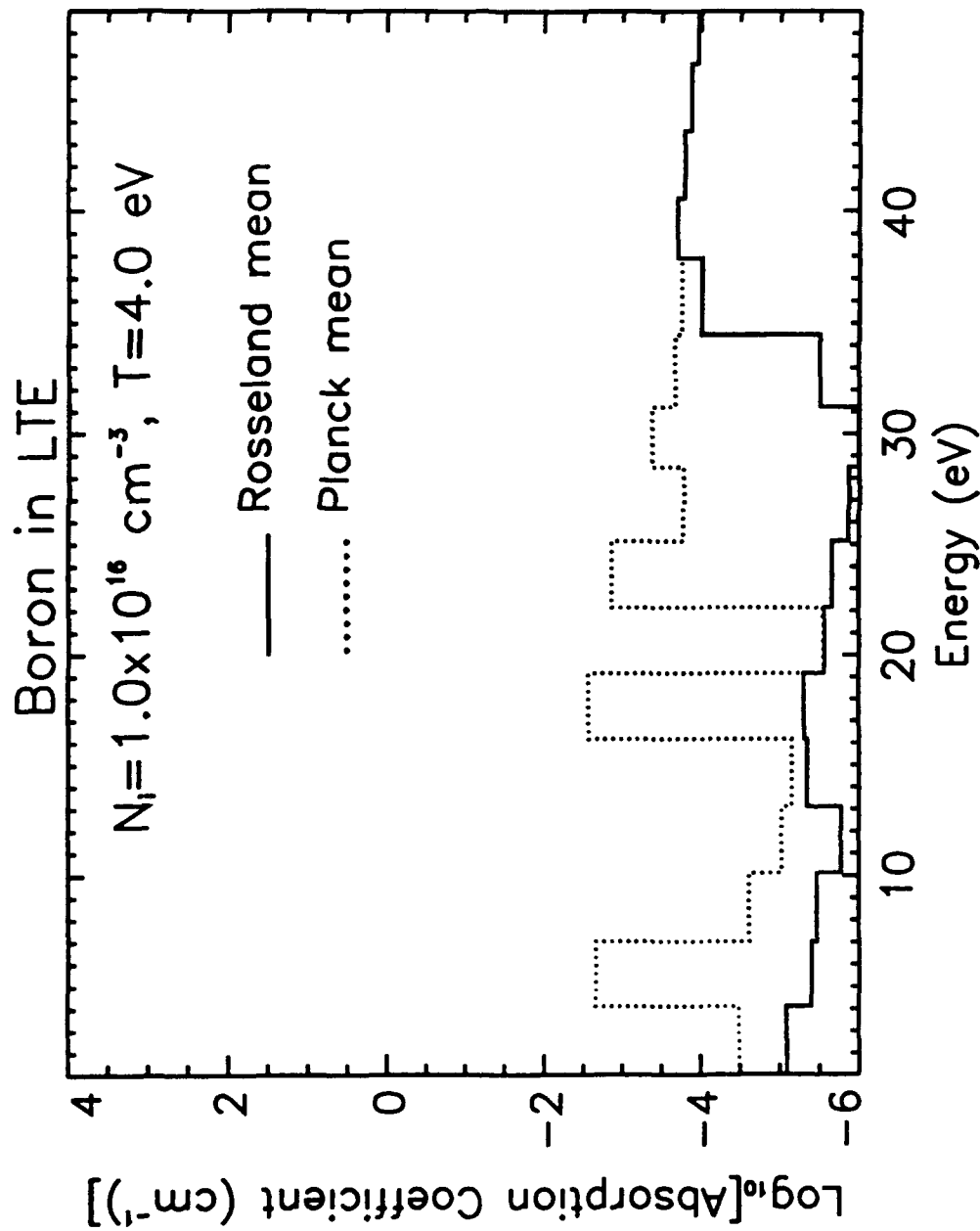FIG. 2. As in Fig. 1, except that the LTE assumption was employed instead of CRE.

FIG. 3. LTE Rosseland and Planck mean opacities for boron are compared for 16 energy bins between 1 and 50 eV, for the same plasma conditions of Figs. 1 and 2.

LOG10(T):																
0.90:	-19.66	-19.46	-20.27	-20.63	-20.81	-19.18	-21.13	-19.63	-20.33	-20.16	-20.42	-20.50	-20.49	-20.58	-20.67	-20.75
0.80:	-19.47	-18.89	-19.95	-20.32	-20.49	-18.58	-20.82	-19.00	-19.76	-19.54	-19.80	-19.89	-19.87	-19.96	-20.05	-20.13
0.70:	-19.25	-18.15	-19.52	-19.96	-19.96	-17.90	-20.43	-18.27	-19.10	-18.80	-19.08	-19.17	-19.13	-19.22	-19.31	-19.39
0.60:	-19.05	-17.40	-18.75	-19.61	-18.96	-17.30	-19.92	-17.59	-18.50	-18.10	-18.41	-18.49	-18.45	-18.53	-18.62	-18.70
0.50:	-18.70	-17.07	-17.74	-19.19	-17.94	-17.16	-19.16	-17.36	-18.34	-17.85	-18.17	-18.24	-18.18	-18.27	-18.36	-18.44
0.40:	-18.26	-17.22	-16.91	-18.74	-17.19	-17.33	-18.44	-17.57	-18.32	-17.98	-18.27	-18.33	-18.30	-18.39	-18.48	-18.56
0.30:	-18.27	-17.94	-16.56	-18.77	-16.96	-17.41	-18.19	-18.23	-18.15	-18.27	-18.32	-18.38	-18.57	-18.66	-18.75	-18.83
0.20:	-18.67	-18.30	-16.51	-19.12	-17.06	-17.51	-18.13	-18.66	-18.10	-18.25	-18.37	-18.50	-18.61	-18.70	-18.79	-18.76
0.10:	-19.18	-17.75	-16.53	-18.91	-17.43	-17.77	-18.33	-19.03	-18.18	-18.34	-18.46	-18.58	-18.32	-18.32	-18.33	-18.39
0.00:	-19.73	-17.40	-16.55	-18.51	-18.15	-18.37	-18.82	-19.34	-18.63	-18.74	-18.35	-18.34	-18.44	-18.39	-18.39	-18.45
-0.10:	-20.37	-17.41	-16.47	-18.39	-18.67	-18.89	-19.14	-19.29	-18.58	-18.67	-18.59	-18.57	-18.68	-18.62	-18.62	-18.68
-0.20:	-21.37	-17.55	-16.39	-18.35	-18.68	-18.95	-18.46	-18.47	-18.45	-18.46	-18.42	-18.40	-18.51	-18.45	-18.45	-18.51
-0.30:	-22.37	-17.78	-16.31	-18.33	-18.66	-18.07	-18.04	-18.10	-18.05	-18.04	-18.07	-18.02	-18.12	-18.07	-18.07	-18.12
-0.40:	-24.03	-18.10	-16.24	-18.30	-17.66	-17.68	-17.64	-17.70	-17.64	-17.65	-17.70	-17.58	-17.72	-17.66	-17.66	-17.72
-0.50:	-25.59	-18.54	-16.16	-17.27	-17.26	-17.28	-17.25	-17.29	-17.24	-17.26	-17.29	-17.19	-17.32	-17.26	-17.26	-17.32
-0.60:	-28.41	-19.14	-15.97	-16.87	-16.86	-16.80	-16.95	-16.88	-16.83	-16.87	-16.88	-16.80	-16.92	-16.86	-16.86	-16.92
-0.70:	-31.55	-19.24	-15.23	-16.47	-16.45	-16.40	-16.56	-16.48	-16.43	-16.48	-16.47	-16.41	-16.52	-16.46	-16.46	-16.52
-0.80:	-35.15	-16.69	-14.83	-16.07	-16.05	-16.00	-16.16	-16.07	-16.02	-16.09	-16.06	-16.01	-16.12	-16.06	-16.06	-16.12
-0.90:	-35.24	-15.15	-14.43	-15.68	-15.65	-15.60	-15.76	-15.67	-15.62	-15.70	-15.65	-15.62	-15.72	-15.66	-15.66	-15.72
-1.00:	-35.13	-14.75	-14.03	-15.28	-15.25	-15.21	-15.12	-15.68	-15.21	-15.31	-15.24	-15.22	-15.32	-15.27	-15.27	-15.32

FIG. 4. Sample of the opacity table for boron. The base 10 logarithm of the Planck mean cross section in cm^2 is stored as a function of electron density and temperature.
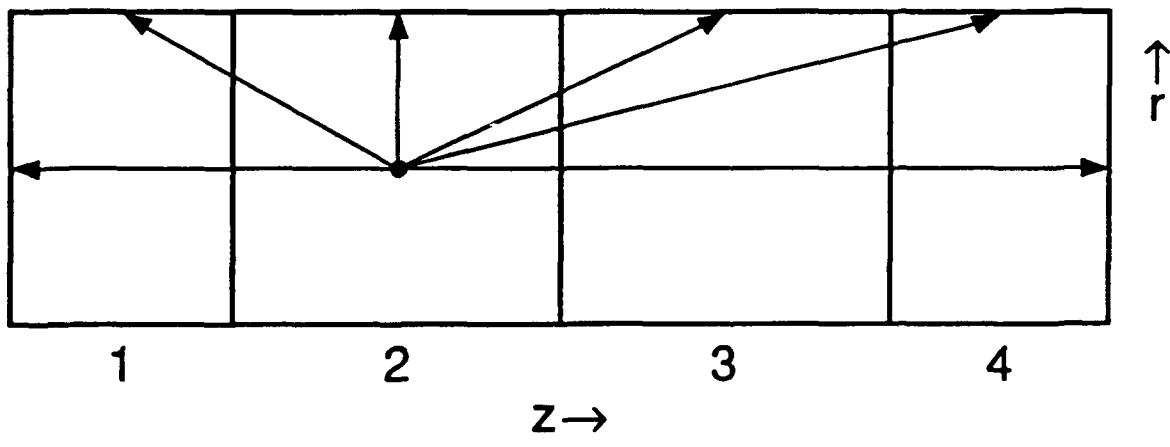
FIG. 5. Ray tracing scheme for quasi-two-dimensional cylindrical radiation transport model. For clarity, only the rays emanating from cell 2 are shown.